Power dissipation in oxide-confined 980-nm vertical-cavity surface-emitting lasers*

Shi Guo-Zhu(史国柱), Guan Bao-Lu(关宝璐)†, Li Shuo(李 硕), Wang Qiang(王 强), and Shen Guang-Di(沈光地)

Key Laboratory of Opto-electronics Technology of Ministry of Education, Beijing University of Technology, Beijing 100124, *China*

(Received 21 May 2012; revised manuscript received 13 June 2012)

We presented 980-nm oxide-confined vertical-cavity surface-emitting lasers (VCSELs) with a 16-μm oxide aperture. Optical power, voltage, and emission wavelength are measured in an ambient temperature range of 5 °C–80 °C. Measurements combined with an empirical model are used to analyse the power dissipation in the device and the physical mechanism contributing to the thermal rollover phenomenon in VCSEL. It is found that the carrier leakage induced self-heating in the active region and the Joule heating caused by the series resistance are the main sources of power dissipation. In addition, carrier leakage induced self-heating increases as the injection current increases, resulting in a rapid decrease of the internal quantum efficiency, which is a dominant contribution to the thermal rollover of the VCSEL at a larger current. Our study provides useful guidelines to design a 980-nm oxide-confined VCSEL for thermal performance enhancement.

Keywords: vertical-cavity surface-emitting lasers, power dissipation, thermal rollover

PACS: 42.55.Px, 42.60.Lh, 42.72.Ai **DOI:** 10.1088/1674-1056/22/1/014206

1. Introduction

The vertical-cavity surface-emitting laser (VCSEL) has become an efficient power light source in optical storage, gas detection, high bit-rate date transmission, optical interconnection, and supercomputing, due to its advantages, such as low cost, low power consumption, small size, single longitude mode operation, and high speed modulation.[1–8] The 980-nm VCSEL has usually been used for pumping the solid-state and fiber laser.[9,10] In recent years, great progress has been achieved in this field, and there have been extensive applications in short distance optical networks.[11,12] In addition, the substrate of GaAs material of the laser is transparent at 980 nm, and the wavelength of 980 nm is desirable for Si-based photodetectors, since the absorption coefficient of Si is much larger at 980 nm than at a longer wavelength. Due to large detuning between the quantum well (QW) photoluminescence peak and the cavity resonance design, excellent temperature stability is obtained. Such advantages make the 980-nm VCSEL a potential competitor to 850-nm VCSEL in short distance data transmission applications. However, both static and dynamic characteristics of the VCSEL are limited by its thermal performance.[13,14] The main hurdle to improving the thermal performance of the VCSEL is current induced self-heating. Under a continuous wave (CW), the self-heating effect leads to the thermal rollover of the optical power with the increase of current. Previous work has been performed to improve the self-heating effect by reducing series resistance.[15–17] However, it is important to understand the interaction among various power dissipation mechanisms and the key contributor to the saturation of the output power with increasing injection current.

In this paper, an oxide-confined 980-nm VCSEL with a 16-μm oxide aperture is presented. The optical power, voltage drop, and emission wavelength are measured as a function of the injection current in an ambient temperature range of 5 °C–80 °C under continuous wave operation. Threshold current, slop efficiency, series resistance, dissipated power, thermal impedance, and internal quantum efficiency of the VCSEL are extracted from the measurements. An empirical model[18] is used to analyse various variations of power dispassion as the injection current increases. From the empirical modeling, power dissipation is divided by linear power dissipation induced by absorption in resonance cavity, spontaneous recombination, carrier thermalization, carrier leakage in the active region, and quadratic power dissipation, such as Joule heating caused by series resistance. It is found that carrier leakage induced power dissipation is responsible mainly for thermal rollover in VCSEL at a larger injection current. Our analysis provides an insight into VCSEL design optimization for improving the thermal performance.

2. Device structure and fabrication

The epitaxial layers were grown on n-type GaAs substrates by metal organic vapour phase epitaxy (MOVPE), as shown in Fig. 1(a). The $Al_{0.9}Ga_{0.1}As/Al_{0.12}Ga_{0.88}As$ distributed Bragg reflectors (DBRs) with a 20-nm-thick linearly graded interface, as well as 23 and 36 pairs, were used as p-doped top and n-doped bottom mirrors, respec-

*Project supported by the National Natural Science Foundation of China (Grant Nos. 60908012 and 61076148) and the Foundation of Beijing Municipal Education Commission, China (Grant No. KM201010005030).

†Corresponding author. E-mail: gbl@bjut.edu.cn

© 2013 Chinese Physical Society and IOP Publishing Ltd

tively. The un-doped active region consists of three 6-nm-thick $In_{0.17}Ga_{0.83}As$ QWs separated by a 4-nm-thick $GaAs_{0.92}P_{0.08}$ barrier between the two QWs, with a photoluminescence (PL) peak at 971 nm. A 30-nm-thick $Al_{0.98}Ga_{0.02}As$ oxidization layer was positioned above the active region for current and optical confinement. Graded interfaces and modulation doping were used on the top and bottom DBR layer to reduce the differential resistance, while maintaining a low free carrier absorption loss.

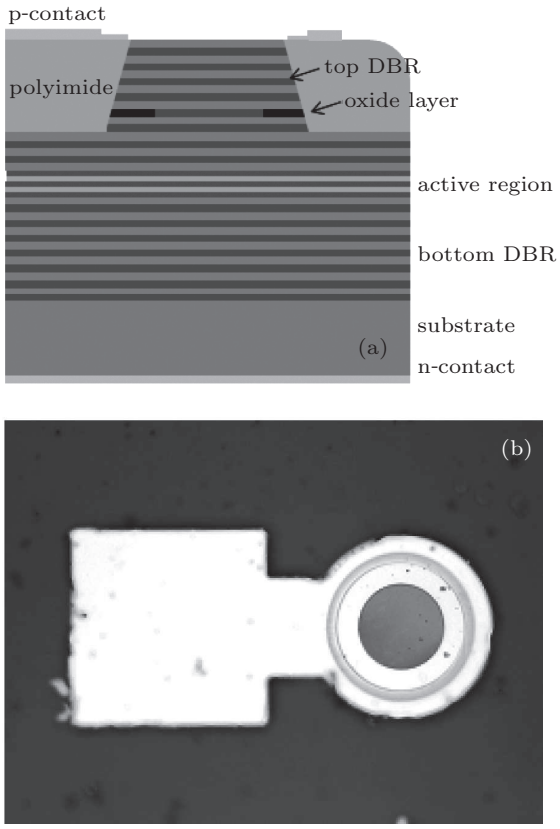


Fig. 1. (a) Schematic cross-section of the VCSEL. (b) Microscope image of the fully processed VCSEL on wafer.

Photolithography and wet etching technology were used to fabricate the VCSEL. A circular mesa was formed by wet etching to a depth under the $Al_{0.98}Ga_{0.02}As$ oxide-confined layer. The etchant was prepared from the mixture of the methanol phosphoric acid hydrogen peroxide and DI water with a volume ratio of 1:3:1:5, and cooled in ice–water mixture for half an hour. The etching process took about 6 min with 600 nm/min average rate in ice–water mixture environment. After the $Al_{0.98}Ga_{0.02}As$ oxide-confined layer was exposed to wet etching, the thermal oxidation was carried out at 450 °C by bubbling nitrogen in heated water of 95 °C. Then, the mesa was planarized using polyimide. After the thickness reached 350 nm, Ti–Au and Au–Ge–Ni–Au were deposited as p-type and n-type ohmic contacts on the top planarized mesa, respectively. Finally a subsequent annealing process was performed to give an ohmic contact. The microscope image of the VCSEL is shown in Fig. 1(b).

3. Device measurements

The measurement is performed in an ambient temperature range of 5–80 °C. The VCSEL wafer is placed on a copper heat sink using a Peltier element as a thermistor by controlling the ambient temperature. The optical power is measured by PIN photodiode, and the spectrum measurement is

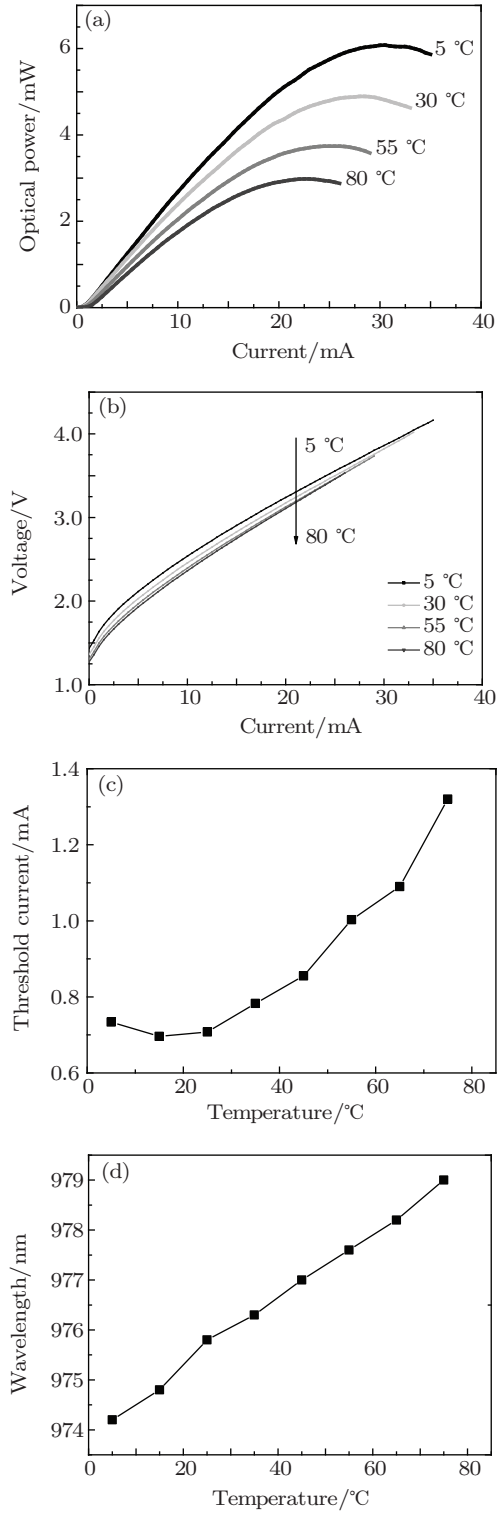


Fig. 2. (a) Measured optical power and (b) voltage as functions of injection current at four different ambient temperatures under CW operation; (c) threshold current and (d) emission wavelength as functions of ambient temperature.

performed by coupling the laser into a multi-mode fiber (MMF), which is connected to a spectrum optical analyzer (SOA). Measurements at different ambient temperatures are illustrated in Fig. 2.

In Fig. 2(a), the VCSEL is the thermal rollover at a lower injection current as the ambient temperature increases. The voltage drop decreases with increasing ambient temperature (see Fig. 2(b)), which is attributed to a reduction of band gap and improvement of carrier transportation through the multi-layer structure. Figure 2(c) clearly shows that the minimum of the threshold current occurs at 15 °C, with gain peak aligned with the cavity resonance.[19] Figure 2(d) shows the variation of emission wavelength with ambient temperature. The measurement is performed near the lasing threshold to avoid self-heating effect. The wavelength shift with temperature $(\Delta\lambda/\Delta T)$ is measured to be 0.068 nm/°C.

4. Empirical modeling and discussion

The total power dissipation in a VCSEL can be divided into quadratic power dissipation (QPD) and linear power dissipation (LPD), which quadratically and linearly depend on injection current ($I_{\rm in}$), respectively. The quadratic power dissipation is caused by series resistance ($R_{\rm s}$) which generates Joule heating. The dependence of power dissipation on the injection current is quadratic, which can be written as

$$P_{\rm diss} = P_{\rm QPD} + P_{\rm LPD}, \tag{1}$$

$$P_{\rm QPD} = I_{\rm in}^2 R_{\rm s}(T_{\rm a}, I_{\rm in}), \tag{2}$$

where $T_{\rm a}$ is the ambient temperature, $R_{\rm s}$ is the series resistance, which depends on the ambient temperature and injection current. The linear power dissipation caused by various mechanisms includes carrier leakage ($P_{\rm leak}$), carrier thermalization ($P_{\rm thermal}$), spontaneous carrier recombination in active region ($P_{\rm recom}$) and absorption in the resonance cavity ($P_{\rm abs}$), and it is expressed as[18]

$$P_{\rm LPD} = K(T)I_{\rm in} = P_{\rm leak} + P_{\rm thermal} + P_{\rm recom} + P_{\rm abs}, \tag{3}$$

where $K(T)$ is the LPD coefficient which depends on the device temperature, ambient temperature, and injection current. The device temperature is the sum of the ambient temperature and the injection current induced self-heating (temperature rise) in the device. To better understand the $P_{\rm LPD}$ modeling, it is significant to analyse the interaction between various physical processes behind each of the constituent LPD mechanisms. Figure 3 illustrates the behaviour of carriers in the active region of the VCSEL. In the figure, $E_{\rm B}$ and $E_{\rm L}$ are the temperature-dependent barrier energy band-gap and laser photon energy in quantum well, respectively; $\eta_{\rm inter}$ is the internal quantum efficiency; $\eta_{\rm inter}I_{\rm in}$ denotes the fraction of injection current captured by the quantum well; $(1-\eta_{\rm inter})I_{\rm in}$ represents the remaining carriers leaking out of active region.

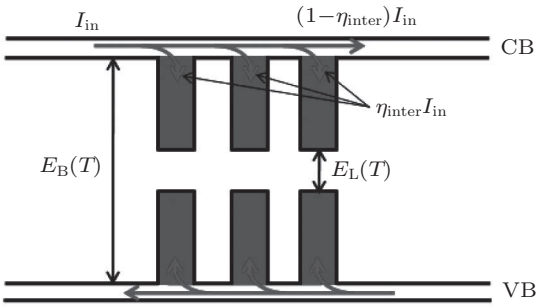


Fig. 3. Schematic illustration of the capture and leakage of injection carriers in quantum wells.

$GaAs_{0.92}P_{0.08}$ is used for a barrier in the active region. The temperature dependence of the barrier band-gap is determined by Varshini equations[20] for the temperature dependence on the band-gap of GaP and GaAs as follows:

$$E_{\rm g}({\rm GaP}) = 2.72 - \frac{0.5771\times10^{-3}\times T_{\rm k}^2}{T_{\rm k}+372}, \tag{4}$$

$$E_{\rm g}({\rm GaAs}) = 1.519 - \frac{0.5405\times10^{-3}\times {\rm T}_{\rm k}^2}{{\rm T}_{\rm k}+204}, \tag{5}$$

where $T_{\rm k}$ is the device temperature in Kelvin. The barrier band-gap of $GaAs_xP_{1-x}$ is written as

$$E_{\rm g}^x({\rm GaAs}_x P_{1-x}) = xE_{\rm g}({\rm GaAs}) + (1-x)E_{\rm g}({\rm GaP}) - x(1-x)C. \tag{6}$$

The bowing parameter C is 0.16 eV for $GaAs_xP_{1-x}$ material.[20] The internal quantum efficiency is defined as the fraction of charge carriers captured by quantum wells, which transform into photons by stimulated emission. The rest of remaining carries are composed of carrier leakage, recombination in the barriers, which includes $P_{\rm leak}$. The $P_{\rm thermal}$ is produced by scattering in quantum wells.[21] The $P_{\rm rec}$ is the power dissipation caused by the heat of spontaneous recombination. The $P_{\rm abs}$ is the power dissipation induced by internal optical loss in the resonance cavity. Various power dissipations can be written as follows:[18]

$$P_{\rm leak} = E_{\rm B}[1-\eta_{\rm inter}(T)]I_{\rm in}/q, \tag{7}$$

$$P_{\rm thermal} = [E_{\rm B}(T) - E_{\rm L}(T)]\eta_{\rm inter}(T)I_{\rm in}/q, \tag{8}$$

$$P_{\rm rec} = E_{\rm L}(T)\eta_{\rm inter}(T)I_{\rm b}/q, \quad I_{\rm b} < I_{\rm th}, \tag{9}$$

$$P_{\rm rec} = E_{\rm L}(T)\eta_{\rm inter}(T)I_{\rm th}(T)/q, \quad I_{\rm b} > I_{\rm th}, \tag{10}$$

$$P_{\rm abs} = \frac{\eta_{\rm inter}(T)[I_{\rm b}-I_{\rm th}(T)][\alpha_{\rm in}(T)+\alpha_m^{\rm B}(T)]E_{\rm L}(T)}{q[\alpha_m^{\rm B}(T)+\alpha_m^{\rm T}(T)+\alpha_{\rm in}(T)]}, \quad I_{\rm b} > I_{\rm th}, \tag{11}$$

$$E_{\rm L}(T) = hc/\lambda(T), \tag{12}$$

where q is the electron charge, $I_{\rm th}$ denotes the threshold current, c is the speed of light and h represents the Planck constant, λ(T) is the emission wavelength as a function of device temperature, $\alpha_{\rm m}^{\rm B}(T)$ and $\alpha_{\rm m}^{\rm T}(T)$ are the transmission loss through the bottom and top DBR, respectively, and $\alpha_{\rm in}(T)$ denotes the internal optical loss in the resonance cavity. In Eq. (11), $P_{\rm abs}=0$, the injection current, is below the threshold current. The device temperature is obtained by the thermal impedance $R_{\rm th}$, which relates to the change in device temperature to the power dissipation and can be written as[22]

$$T = T_{\rm a} + \Delta T = T_{\rm a} + R_{\rm th} P_{\rm diss}, \tag{13}$$

where ΔT is the temperature increment caused by the injection current induced self-heating, $R_{\rm th}$ is the thermal impedance of the device, which is defined as the ratio of the temperature increment to the variation of the dissipated power and can be written as[16]

$$R_{\rm th} = \frac{\Delta T}{\Delta P_d} = \frac{(\Delta\lambda/\Delta P_{\rm diss})}{(\Delta\lambda/\Delta T)}. \tag{14}$$

An indirect method is used to obtain the thermal impedance. The emission wavelengths are measured at different ambient (copper heat sink) temperatures as the injection current is near the threshold in order to remove the self-heating effect. The change of the emission wavelength as a function of power dissipation ($\Delta\lambda/\Delta P_{\rm d}$) is obtained using the measurements of the emission wavelength and optical power at various continuous injection currents. The thermal impedance is calculated to be 1.029 °C/mW at 55 °C from extracted measurements, which agrees well with the dimensional dependence of thermal impedance following a simple analytical expression $R_{\rm th}=1/(\xi d)$,[23] where d is the oxide aperture diameter, and ξ denotes the effective thermal conductivity. Equation (13) can be used to estimate the device temperatures at various ambient temperatures and injection currents. The internal quantum efficiency is calculated with slope efficiency (SE) and external quantum efficiency ($\eta_{\rm d}$). The external quantum efficiency is written as[24]

$$\eta_{\rm d}(T) = \frac{q\lambda(T)}{hc} SE(T). \tag{15}$$

The relationship between internal quantum efficiency and external efficiency is

$$\eta_{\rm inter}(T) = \frac{(\alpha_{\rm m}^{\rm B}(T) + \alpha_{\rm m}^{\rm T}(T) + \alpha_{\rm in}(T))\eta_{\rm d}(T)}{\alpha_{\rm m}^{\rm T}(T)}. \tag{16}$$

The series resistance and power dissipation are extracted from the measurements, which have shown in Figs. 4(a) and 4(b), respectively. The series resistance rapidly decreases as the injection current increases, because of the increase in charge accumulation on the DBR interface with increasing injection current.[25] The power dissipation is obtained by $P_{\rm diss}=I_{\rm in}V-P_{\rm optical}$, which can be calculated from measurements. Device temperatures are calculated at different ambient temperatures in a range of 5–80 °C in Fig. 4(c). The temperature in the VCSEL is higher than the ambient temperature, owing to the self-heating induced by the injection current. With the slope efficiencies extracted from measurements at different ambient temperatures, the internal efficiency is calculated and numerically fitted by Eqs. (15) and (16) in Fig. 4(d). It is clearly shown that as the injection current increases, the internal quantum efficiency declines, especially at a high ambient temperature (80 °C).

The LPD and QPD can be calculated with the equations mentioned in the empirical modeling. The LPD coefficient $K(T)$ can be divided into a few parts of including the coefficient of carrier leakage ($K_{\rm leak}$), carrier thermalization ($K_{\rm thermal}$), spontaneous carrier recombination in active region ($K_{\rm recom}$) and absorption in the resonance cavity ($K_{\rm abs}$). Figure 5(a) shows the curves of the LPD coefficient versus the injection current at four different ambient temperatures. Four curves show that at the beginning, values of K decrease rapidly as injection current increases and reach their minimum value, and then slowly increase with increasing current, until the thermal rollover occurs. The increase of K makes a rapid increase in device temperature, which eventually causes thermal rollover. In Fig. 5(b), the threshold currents, each as a function of injection current, are calculated at four different temperatures. Because of the self-heating induced by injection current, the temperature in the VCSEL increases, therefore, the threshold current increases with increasing injection current. Figure 5(c) displays the total LPD coefficient and individual coefficients versus injection current for the four LPD physics processes at 80 ^{o}C. The LPD coefficient K is the sum of the four individual LPD coefficients. The results of the individual Kparameters, as a function of injection current, are calculated from Eqs. (7)–(11).

The thermalization LPD coefficient is almost constant and the carrier leakage LPD coefficient is fairly larger than the other three LPD coefficients over a large range of injection current. Because there is no internal optical loss below the laser threshold, the absorption LPD coefficient is close to zero. The heating is mostly generated by spontaneous recombination, therefore, the recombination LPD coefficient is at a very high value. As the injection current increases, the spontaneous recombination is replaced by stimulated emission, therefore, the recombination LPD coefficient decreases. At the same time, the absorption of photons induced internal optical loss in the resonance cavity increases, and hence the absorption LPD coefficient increases. The LPD coefficient of the carrier leakage increases rapidly close to the range of the injection current corresponding to the thermal rollover. From Eq. (7), we can see that the increase of the carrier leakage LPD coeffi-

cient is due to the reduction of the internal quantum efficiency plotted in Fig. 4. Figure 5(d) shows various individual LPDs corresponding to the LPD coefficients in Fig. 5(c). The carrier leakage induced LPD is much larger than the others over a large range of injection current, it is the main source of heating contributing to thermal rollover in VCSEL. With the injection current increasing, the carrier leakage induced LPD increases, especially close to the injection current corresponding to the thermal rollover. This is due to the rapid reduction of the internal quantum efficiency at a larger current just mentioned above. Other two individual LPDs are fairly constant over the range of injection current and have little contribution to the total LPD.

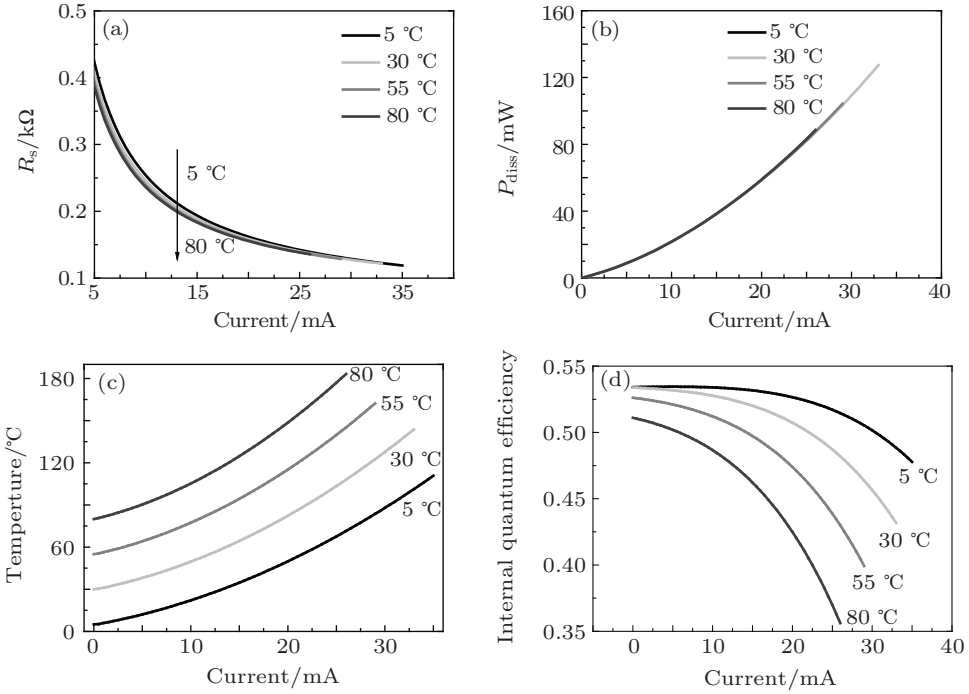


Fig. 4. Curves of (a) series resistance, (b) power dissipation, (c) device temperature, and (d) internal quantum efficiency versus injection current at four different ambient temperatures.

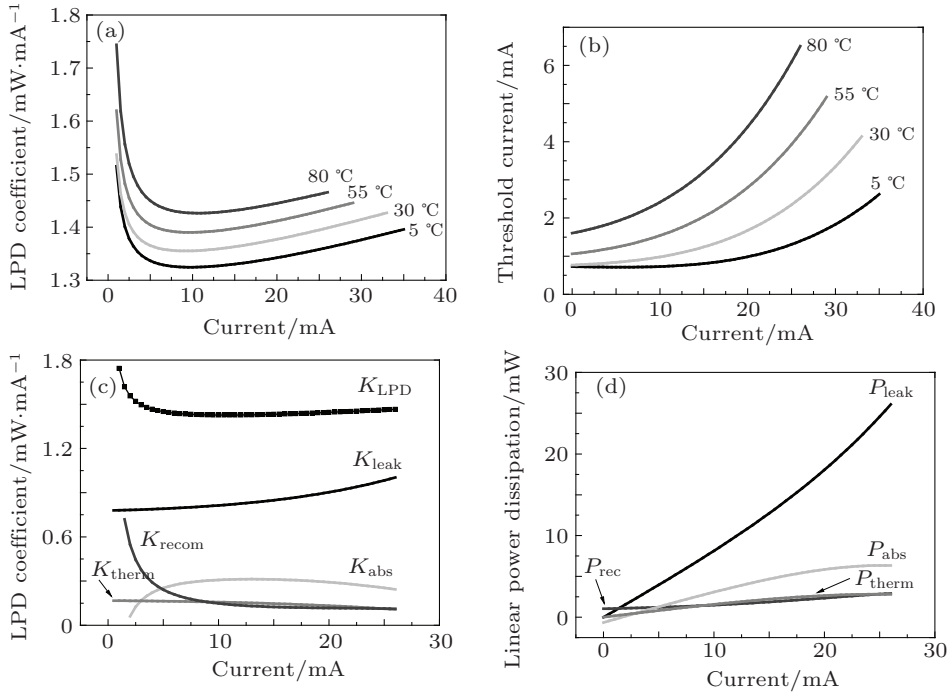


Fig. 5. Curves of (a) LPD coefficient K and (b) threshold current versus injection current at four different temperatures; curves of (c) LPD coefficients K and (d) LPD versus injection current at 80 °C.

5. Conclusion

980-nm oxide-confined VCSELs with a 16-μm inner aperture are presented in this paper, and the thermal behavior and various thermal rollover mechanisms are analyzed in detail with the aid of an empirical model. Parameters used in the empirical modeling are extracted from the measurements of the optical power, voltage drop, and emission wavelength as functions of injection current at different ambient temperatures in the range of 5–80 °C. The thermal impedance measured using an indirect method is 1.029 °C/mW at the ambient temperature of 55 °C. The LPD specially analysed in this model shows that the carrier leakage induced power dissipation is the dominant contribution to the LPD among various individual LPDs. Furthermore, thermal rollover behavior is caused by a rapid reduction of the internal quantum which results from the increase of carrier leakage induced power dissipation at the larger injection current. The current induced self-heating leads to the temperature increase in the VCSEL. The careful analysis of the various power dissipation mechanisms contributing to the thermal saturation of the device can provide significant guidance for improving the VCSEL design to include a good thermal performance.

References

[1] Hofmann W, Moser W, Wolf P, Mutig A, Kroh M and Bimberg D 2011 *Optical Fiber Communication Conference* March 6, 2011 Los Angeles, USA, p. PDPC5

[2] Liu A J, Qu H W, Chen W, Jiang B, Zhou W J, Xing M X and Zheng W H 2011 *Chin. Phys.* B **20** 024204

[3] Anan T, Suzuki N, Yashiki N, Fukatsu K, Hatakeyama H, Akagawa T, Tokutome K and Tsuji M 2008 *Optical Fiber Communication/National Fiber Optic Engineer Conference* February 24–28, 2008 San Diego, USA, p. 1

[4] Guan B L, Ren X J, Li C, Li S, Shi G Z and Guo X 2011 *Chin. Phys.* B **20** 094206

[5] Chang Y C, Wang C and Coldren L A 2007 *Electron. Lett.* **43** 1022

[6] Lin C K, Tandon A, Djordjev K, Corzine S and Tan M 2007 *IEEE J. Select. Topics Quantum Electron.* **13** 1332

[7] Zhang W L, Pan W, Luo B, Li X F, Zou X H and Wang M Y 2008 *Chin. Phys.* B **17** 1821

[8] Schow C, Doany F and Kash J 2010 *IEEE Spectrum* **47** 32

[9] Goldberg L, Mclntosh C and Cole B 2011 *Opt. Express* **19** 4261

[10] Wu J and Summer H D 2009 *Chin. Phys.* B **18** 4912

[11] Chang Y C and Coldren L A 2009 *IEEE J. Select. Topics Quantum Electron.* **15** 704

[12] Mutig A, Lott J A, Blokhin S A, Wolf P, Moser P, Hofmann W, Nadtochiy A M, Payusov A and Bimberg D 2010 *Appl. Phys. Lett.* **97** 151101

[13] Ding Y, Fan W J, Xu W, Tong C Z, Liu Y and Zha L J 2010 *Appl. Phys.* B **98** 773

[14] Mutig A, Fiol G, Moser P, Arsenijevic D, Shchukin V A, Hopfer F and Bimberg D 2008 *Electron. Lett.* **44** 1305

[15] Omari A and Lear K 2004 *IEEE Photon. Technol. Lett.* **16** 969

[16] Westbergh P, Gustavsson S, Haglund A, Skold M, Joel A and Larsson A 2009 *IEEE J. Select. Topics Quantum Electron.* **15** 649

[17] Li T, Ning Y Q, Hao E J, Cui J J, Zhang Y, Liu G Y, Qin L, Liu Y, Wang L J, Cui D F and Xu Z Y 2009 *Sci. China. Ser.* F **52** 1266

[18] Baveja P, Kogel B, Westbergh P, Gustavsson J, Haglund A, Maywar A, Agrawal G and Larsson A 2011 *Opt. Express* **19** 15490

[19] Sadofev C J, Blumstengel S, Puls S and Henneberger J F 2006 *Appl. Phys. Lett.* **89** 051108

[20] Vurgaftman I, Meye J and Mohan L 2001 *Appl. Phys. Rev.* **89** 5815

[21] Knox W, Chemla D, Livescu G, Cunningham J and Henry J 1988 *Phys. Rev. Lett.* **61** 1290

[22] Mena P, Morikuni J, Kang S, Harton A and Wyatt K 1999 *J. Lightwave Technol.* **17** 865

[23] Coldren L and Corzine S 1995 *Diode Lasers and Photonic Integrated Circuits* (New York: Wiley) pp. 81–83

[24] Wilmsen C, Temkin H and Coldren L 1999 *Vertical-Cavity Surface-Emitting Lasers: Design, Fabrication, Characterization* (New York: Cambridge University Press) pp. 35–36

[25] Chang-Hasnain C, Zah C, Hasnain G, Harbison J, Florez L Stoffel N and Lee T P 1991 *Appl. Phys. Lett.* **58** 1247